Computational Modeling of Hemodynamic Effects in Ventricular Septal Defects: A Multi-model Analysis for Clinical Assessment

Sijie Li[1], Xu Shen[1], Yushan Wei[1]

[1]Department of Biomedical Engineering, Southern University of Science and Technology, Shenzhen, China

This study presents a comprehensive analysis of ventricular septal defects (VSD) using three complementary models: an orifice plate model, a tube model, and a pressure-volume model. We investigated the relationship between VSD size and cardiac hemodynamics to better understand the pathophysiological implications and guide clinical decision-making. The orifice plate model identified a critical defect diameter of 4.4 mm corresponding to a clinically significant pulmonary-to-systemic flow ratio of 1.5. The tube model revealed a nonlinear relationship between defect size and downstream pressure changes, with amplified effects at larger defect diameters. The pressure-volume model demonstrated that VSD diameters exceeding 5 mm led to disproportionate increases in right ventricular pressure.

INTRODUCTION

Ventricular septal defect (VSD) is one of the most common congenital heart diseases, accounting for approximately 20-30% of all congenital cardiac defects.[1,9,13] It is characterized by an abnormal opening in the interventricular septum, resulting in a left-to-right shunt due to the pressure differential between ventricles.[9,13,16] When the pulmonary-to-systemic flow ratio (Q_p/Q_s) exceeds 1.5, the condition becomes hemodynamically significant and may require intervention.[3,15] If left untreated, this persistent shunting can lead to complications including pulmonary hypertension and, in severe cases, Eisenmenger syndrome.[7,12]

The clinical impact of VSD varies substantially with defect size. While small defects may be asymptomatic, larger ones can cause significant complications including heart failure.[14] Despite extensive clinical experience, quantitative understanding of the relationship between defect size and hemodynamic consequences remains incomplete.[6,10] To address this gap, we developed three complementary computational models: an orifice plate model for shunt flow analysis, a tube model for effect on downstream pressure, and a pressure-volume model for ventricular dynamics simulation. This integrated approach aims to provide more quantitative insights into VSD hemodynamics

METHODOLOGY

Orifice Plate Model

The orifice flow model (Figure 1) is used to approximate the shunt flow in cardiac septal defects. The classic formula for the orifice flow model is:

$$Q = c_d A \sqrt{\frac{2\Delta p}{\rho}} \quad (1)$$

where Q is the flow rate through the orifice (i.e., the shunt flow in the cardiac septal defect); cd is the flow coefficient, which is taken as 0.6 based on theoretical analysis and empirical data. A is the effective cross-sectional area of the orifice (i.e., the area of the defect); Δp is the pressure difference across the orifice, taken as 80 mmHg; and ρ is the density of blood, taken as 1.06 g/ml.

The principle of mass conservation is crucial for understanding blood flow distribution in the circulatory system. The blood ejected from the right

ventricle (Q_p) consists of two parts: one part comes from the blood returning from the systemic circulation (Qs), and the other part is the blood shunted through the VSD (Q_c). Based on mass conservation, the following shunt ratio can be calculated:

$$\frac{Q_p}{Q_s} = \frac{Q_s + Q_c}{Q_S} = 1 + \frac{Q_c}{Q_s} \quad 2$$

This ratio is clinically significant: when the ratio is less than 1.5, the hemodynamic effect is considered insignificant; when the ratio is between 1.5 and 2.0, the hemodynamic effect is clinically significant; and when the ratio exceeds 2.0, intervention may be required.

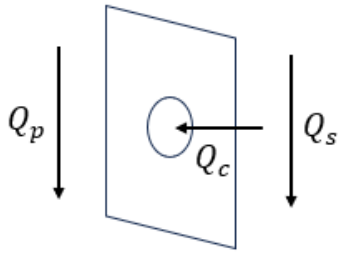

Figure 1. Schematic diagram of the orifice flow model. Q_c is the shunt flow in the cardiac septal defect. Q_p is the blood ejected from the right ventricle. Q_s is the blood returning from systemic circulation.

Tube Mode

To evaluate the effect of defect size on downstream pressure in the right ventricle at varying distances, the two ventricles and the defect are simplified as rigid, uniform, and straight cylindrical tubes, assuming steady, laminar, and incompressible Newtonian blood flow (Figure 2).

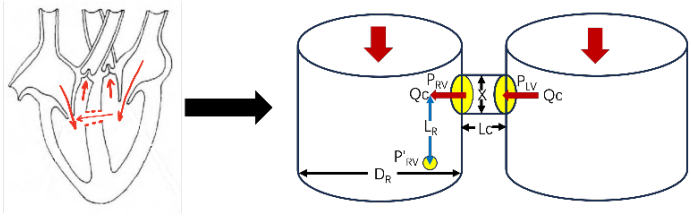

Figure 2: Simplified model of left and right ventricles connected by a defect. This model derives the relationships between the pressure at downstream distances (LR) and defect diameter (x). Known parameters include DR (diameter of the right ventricle), PL and PR (pressures in the left and right ventricles, respectively), and LC (defect length). Yellow areas indicate the locations of pressures. Red arrows represent the direction of blood flow. P'RV denotes the pressure at the downstream location (LR).

With the aforementioned simplifications and assumptions, the governing equations are derived using Poiseuille's law. The resistance of a cylindrical pipe is expressed as[2,8]:

$$R = \frac{128\eta L}{\pi D^4} \quad 3$$

where R is the resistance, L is the pipe length, η is the dynamic viscosity of blood, and D is the pipe diameter. The volumetric flow rate (Q) can then be expressed as[1]:

$$Q = \frac{\Delta p}{R} = \frac{\Delta p \pi D^4}{128\eta L} \quad 4$$

For the defect, the flow rate determined by the pressure difference $P_L - P_R$ across the defect is:

$$Q_c = \frac{(P_L - P_R)\pi x^4}{128\eta L_c} \quad 5$$

Similarly, the change in downstream pressure at L_R is given as:

$$\Delta Q_R = \frac{P_R - P'_{R0}}{R_R} - \frac{P_R - P'_R}{R_R} = \frac{P'_{R0} - P'_R}{128\eta L_R}\pi D_R^4 \quad 6$$

P'_{R0} and P'_R represent the pressures at LR with and without the defect, respectively. By applying flow conservation ($\Delta Q_R = Q_c$), the downstream pressure increment is expressed as:

$$\Delta P_R = P'_R - P'_{R0} = \frac{(P_L - P_R)x^4 L_R}{L_c D_R^4} \quad 7$$

Pressure-volume Model

This model is designed to simulate the overall blood flow in the ventricle, utilizing a regularly moving springboard to mimic the contraction of the myocardium. We hope to obtain the change in ventricular pressure over time. Assumed that all the structures in this model are rigid except the spring. To simplify the calculation, assumed the resistances of the valves are constant. Additionally, the mass of the plate is considered negligible.

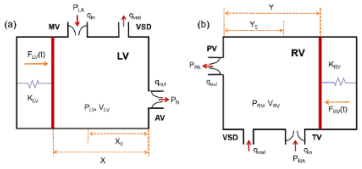

Figure 3. Models of the left and right ventricles. (a) Left ventricle. P_{LV} and V_{LV} are the blood pressure and volume of the left ventricle. q_{in}, q_{out}, q_{vsd} represent the blood flow rates entering through the mitral valve (MV), flowing out through the aortic valve (AV), and exiting through the VSD, respectively. K_{LV} is the elastic coefficient of the spring. $F_{LV}(t)$ is the force exerted by muscle (it is different from the force exerted by the spring and is a function of time). (b) Right ventricle. P_{RV} and V_{RV} are the blood pressure and volume of the right ventricle. q_{in}, q_{out}, q_{vsd} represent the blood flow rates entering through the tricuspid valve (TV), flowing out through the pulmonary artery valve (PV), and entering through the VSD, respectively. K_{RV} is the elastic coefficient of the spring. $F_{RV}(t)$ is the force exerted by muscle.

Taking the isolated left ventricle as an example, by performing a force analysis on the plate, we can derive:

$$P_{LV}A = K_{LV}(X - X_0) + F_{LV}(t) \quad 8$$

Where A is the area of the plate, $(X - X_0)$ is the length of the compressed spring. If we divide both sides of the equation by A and define $\mathrm{E_{LV}} = \frac{\mathrm{K_{LV}}}{\mathrm{A^2}}$ as the elasticity of the left ventricle muscle, which is the volume-dependent elastic coefficient. $\mathrm{V_{LV}} = \mathrm{XA}$ is the volume of the left ventricle, $\mathrm{V_{unlv}} = \mathrm{X_0A}$ is the unstressed volume. The we define $\mathrm{G_{LV}(t)} = \frac{\mathrm{F_{LV}(t)}}{\mathrm{A}}$. We obtain the equation:

$$P_{LV} = E_{LV}(V_{LV} - V_{unlv}) + G_{LV}(t) \quad 9$$

where E_{LV} can be approximated as a constant. ——

For the overall volume of the ventricle:

$$\frac{dV_{LV}}{dt} = q_{in} - q_{out} \quad 10$$

Because the blood flow, q, between the compartments is taken as:

$$q = \frac{P_u - P_d}{R} \quad 11$$

Then we get:

$$\frac{dV_{LV}}{dt} = \frac{P_{LA} - P_{LV}}{R} - \frac{P_{LV} - P_B}{R} - C_d A\sqrt{\frac{2\Delta P}{\rho}} \quad 12$$

where P_{LA} is the blood pressure of left atrium P_B is the blood pressure of human body. R is the resistance of valve. We can differentiate equation (9)：

$$\frac{dP_{LV}}{dt} = E_{LV}\frac{dV_{LV}}{dt} + \frac{dG_{LV}(t)}{dt} \quad 13$$

Distribute equation (13) to equation (12):

$$\frac{dP_{LV}}{E_{LV}dt} + \frac{2}{R}P_{LV} + C_d A\sqrt{\frac{2(P_{LV} - P_{RV})}{\rho}} = \frac{dG_{LV}(t)}{E_{LV}dt} + \frac{P_{LA}}{R} + \frac{P_B}{R} \quad 14$$

For the right ventricle, we apply the same strategy for the calculation:

$$\frac{dP_{RV}}{E_{RV}dt} + \frac{2}{R}P_{RV} - C_d A\sqrt{\frac{2(P_{LV} - P_{RV})}{\rho}} = \frac{dG_{RV}(t)}{E_{RV}dt} + \frac{P_{RA}}{R} + \frac{P_{PA}}{R} \quad 15$$

RESULTS

Orifice Plate Model

Based on the orifice flow model, calculations were made for a shunt flow ratio $Q_p/Q_s = 1.5$, which corresponds to a defect size of approximately 4.4 mm in diameter (Figure 4).

The resulting defect size of 4.4 mm was consistent with the general clinical observation for when a VSD becomes clinically significant in terms of hemodynamic effects.

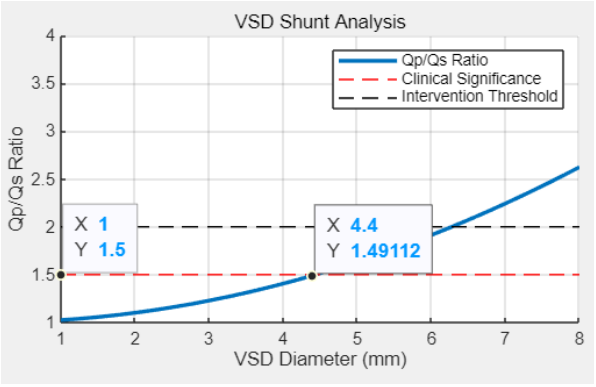

Figure 4: VSD Shunt Flow Analysis Based on the Orifice Flow Model. The figure shows the relationship between the defect diameter and the shunt flow ratio (Q_p/Q_s). The blue solid line represents the calculated results, indicating that the shunt flow ratio increases as the defect diameter increases. Key clinical thresholds are marked: **1.5** (clinical significance) and **2.0** (intervention threshold). The highlighted point X=4.4 mm, Y=1.49112 indicates that when the defect diameter is approximately **4.4 mm**, the shunt flow ratio approaches the clinical significance level of 1.5

Tube Model

By substituting physiological parameters representative of the average adult, $Lc = 8.5mm, D_R = 15mm, P_L = 110mmHg, P_R = 25mmHg$ [4], the relationship between defect diameter (x) and downstream pressure difference (ΔP_R) at various downstream lengths is shown in Figure 5(a).

This analysis identifies a novel hallmark for assessing the impact of defect diameter on right ventricular pressure at specific downstream locations. It aids in determining the need for clinical intervention by evaluating whether the resulting pressure increments pose significant hemodynamic risks. The nonlinear relationship underscores the importance of precise measurement and assessment of larger defects, as small diameter changes can result in disproportionately significant consequences.

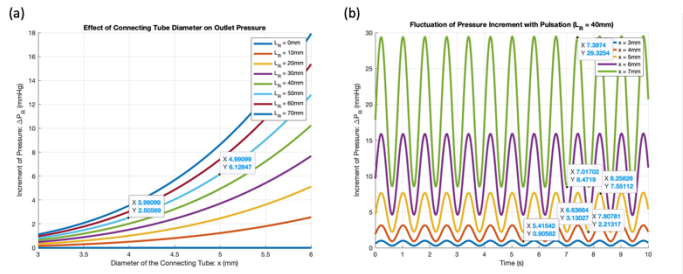

Figure 5: **(a)** Downstream pressure difference (ΔPR) as a function of defect diameter (x). The relationship between the pressure increment (ΔPR) and the connecting tube diameter (x) demonstrates a strong nonlinearity, governed by a fourth-power dependence on x. As a result, the pressure increment increases sharply as x becomes larger. Furthermore, the pressure increment grows proportionally with the distance downstream from the defect (LR), indicating the compounding effects of spatial separation. **(b)** Fluctuation of Pressure Increment with time variant Pulsation (LR = 40mm). It is observed that as the defect diameter (x) increases, both the mean pressure increment and the amplitude of fluctuation increase significantly.

To simulate cardiac pulsation, sinusoidal functions with empirical parameters (equation (16) and (17)) are applied.

$$p_{LV}(t) = 65 + 55sin(7.85t) \quad 16$$

$$p_{LV}(t) = 65 + 55sin(7.85t) \quad 17$$

The results in Figure 5 provide a dynamic representation of the pressure increment (ΔP_R) during cardiac pulsation, showing how it increases on average and exhibits amplified oscillatory behavior with larger defect diameters (x). Clinically, this temporal information enables more accurate assessment when correlated with empirical data, such as electrocardiograms (ECG) and pressure measurements, to identify hemodynamic patterns.

Pressure-Volume Model

By combining equations (8) and (9), we obtain a system of partial differential equations, where $\frac{dG_{LV}(t)}{dt} = 113.75\pi sin\frac{\pi t}{0.4}$, $\frac{dG_{RV}(t)}{dt} = 25.25\pi sin\frac{\pi t}{0.4}$, E_{LV} is equal to 0.1 and E_{RV} is equal to 0.07[5]. And after approximating the valve resistance, we can obtain $R = 0.04$. P_{RA}, P_{PA}, P_{LA} and P_B are equal to 100 mmHg, 20 mmHg, 100 mmHg and 20mmHg, respectively. Set the initial value of P_{LV} and P_{RV} as 110 mmHg and 25 mmHg. To analyze how blood pressure changes with the size of the VSD, we set the VSD diameters to 0, 4, 5, and 10, and use MATLAB to solve the system of equations to calculate the ventricular pressures corresponding to each A value. The results are as follow:

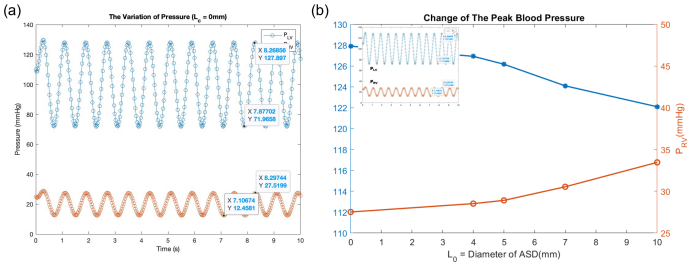

Figure 6: (a) The change of blood pressure with respect to time in left and right ventricles. **(b)** Peak blood pressure of left and right ventricles at different diameters of VSD

It can be seen that after the VSD diameter exceeds 5 mm, the right ventricular pressure increases at a faster rate compared to before 5 mm.

LIMITATIONS

Several important limitations exist in our model construction process. In the orifice plate model, we simplified the ventricular septal defect as a perfect circular opening, neglecting the dynamic characteristics of cardiac pressure variations and the influence of vascular elasticity on flow patterns. The tube model assumes blood flow to be steady, laminar, and an incompressible Newtonian fluid, which may not fully represent the complex pulsatile and turbulent nature of cardiac blood flow. This simplification also overlooks ventricular wall compliance and non-Newtonian blood properties, factors that could significantly impact hemodynamic behavior. In the pressure-volume model, we simplified several cardiac properties, including treating valve resistance as a constant value when it actually varies with valve opening and closing, using a basic sinusoidal function to simulate myocardial contractility rather than more physiologically accurate piecewise functions, and basing myocardial wall elastic coefficients solely on empirical estimates.

Many parameters used in the models rely on empirical values or generalizations, including flow coefficients in the orifice model, blood viscosity parameters, ventricular elastic coefficients, and valve resistance values, which may not accurately reflect individual patient variations. Furthermore, there is

currently no established clinical threshold for determining when pressure increments (ΔP_R) reach levels requiring clinical intervention, which somewhat limits the direct clinical applicability of the tube model findings.

PROSPECTS

Future developments in this research field can proceed in several key directions. The primary task is to enhance the physiological accuracy of existing models. For the orifice plate model, future improvements can focus on incorporating vascular wall elasticity and considering the pulsatile nature of blood flow, while optimizing the selection of flow coefficients through more extensive clinical data. Regarding the tube model, we will emphasize the introduction of more realistic boundary conditions and flow dynamics, particularly establishing clinical intervention thresholds for pressure increments (ΔP_R). This will require correlation studies between simulation results and clinical data, utilizing meta-analysis and large-scale data integration approaches to investigate the relationship between pressure increments and physiological damage, thereby providing more objective criteria for clinical decision-making. For the pressure-volume model, future work will concentrate on implementing more precise functions for valve resistance and myocardial contractility, specifically using piecewise functions that can accurately capture variations during cardiac contraction and relaxation phases to better simulate cardiac dynamics.

Through these improvements, each model will be optimized and refined in its specific research direction. These more accurate models will provide more reliable theoretical foundations for clinical practice, helping physicians make more precise decisions in treating ventricular septal defects. Meanwhile, the improved models will also serve as more powerful research tools for further understanding cardiac hemodynamic mechanisms.

CONCLUSION

This study presents a comprehensive multi-model analysis of ventricular septal defects, providing quantitative insights into the relationship between defect size and hemodynamic consequences. Through the orifice plate model, we identified a critical defect diameter of 4.4 mm corresponding to a clinically significant pulmonary-to-systemic flow ratio of 1.5, offering an objective reference point for clinical assessment. The tube model revealed the nonlinear relationship between defect size and downstream pressure changes, demonstrating that larger defects can lead to disproportionate increases in pressure gradients. Furthermore, the pressure-volume model illustrated that VSD diameters exceeding 5 mm result in accelerated increases in right ventricular pressure, suggesting a potential threshold for clinical intervention.

The integration of these three complementary models provides a more complete understanding of VSD hemodynamics than any single model alone. While each model focuses on different aspects of the defect's impact, together they offer a comprehensive framework for evaluating the severity and potential consequences of VSDs. The findings not only contribute to the theoretical understanding of VSD pathophysiology but also provide practical guidance for clinical decision-making. Despite current limitations, this study establishes a foundation for future research in computational modeling of congenital heart defects and demonstrates the potential of multi-model approaches in advancing our understanding of complex cardiac conditions.

REFERENCE

[1]Ethier, C. R., & Simmons, C. A. (2007). Introductory biomechanics: From cells to organisms. Cambridge University Press.

[2]Fox, R. W., McDonald, A. T., & Pritchard, P. J. (2011). Introduction to fluid mechanics (8th ed., SI version). John Wiley & Sons, Inc.

[3]Feltes, T. F., et al. (2021). Indications for cardiac catheterization and intervention in pediatric cardiac disease: A scientific statement from the American Heart Association. Circulation, 123(22), 2607-2652. https://doi.org/10.1161/CIR.0b013e31821b1f10

[4]Henry, W. L., DeMaria, A., Gramiak, R., King, D. L., Kisslo, J. A., Popp, R. L., & Sahn, D. J. (1980). Report of the American Society of Echocardiography Committee on Nomenclature and Standards in Two-dimensional Echocardiography. Circulation, 62(2), 212-217.

[5]Noreen, S., Ben-Tal, A., Elstad, M., Sweatman, W. L., Ramchandra, R., & Paton, J. (2022). Mathematical modelling of atrial and ventricular pressure-volume dynamics and their change with heart rate. Mathematical biosciences, 344, 108766. https://doi.org/10.1016/j.mbs.2021.108766

[6]Penny, D. J., et al. (2022). Ventricular septal defect. The Lancet, 377(9771), 1103-1112.

[7]van der Linde, D., Konings, E. E. M., Slager, M. A., Witsenburg, M., Helbing, W. A., Takkenberg, J. J. M., & Roos-Hesselink, J. W. (2011). Birth prevalence of congenital heart disease worldwide: A systematic review and meta-analysis. Journal of the American College of Cardiology, 58(21), 2241-2247. https://doi.org/10.1016/j.jacc.2011.08.025

[8]Westerhof, N., Stergiopulos, N., & Noble, M. I. M. (2010). Snapshots of hemodynamics: An aid for clinical research and graduate education (2nd ed.). Springer.

[9]American Society of Echocardiography, & European Association of Cardiovascular Imaging. (2015). Recommendations for cardiac chamber quantification by echocardiography in adults: An update from the American Society of Echocardiography and the European Association of Cardiovascular Imaging. Journal of the American Society of Echocardiography, 28(1), 1-39. https://doi.org/10.1016/j.echo.2014.10.003

[10]Ben-Tal, A., Elstad, M., Noreen, S., Paton, J., Ramchandra, R., & Sweatman, W. L. (2022). Mathematical modelling of atrial and ventricular pressure-volume dynamics and their change with heart rate. Mathematical Biosciences, 344, 108766. https://doi.org/10.1016/j.mbs.2018.108766

[11]Eckerström, F., Nyboe, C., Maagaard, M., Redington, A., & Hjortdal, V. E. (2023). Survival of patients with congenital ventricular septal defect. European Heart Journal, 44(1), 54-61.

[12]Gupta, S. S., & Sinha, A. (2016). Ventricular septal defect. QJM: An International Journal of Medicine, 109(10), 691–692. https://doi.org/10.1093/qjmed/hcw112

[13]Phillips, G., & Others, A. (1977). Health instruction packages: Cardiac anatomy. Retrieved from https://www.proquest.com/encyclopedias-reference-works/health-instruction-packages-cardiac-anatomy/docview/63617137/se-2

[14]Nayak, S., Patel, A., Haddad, L., Kanakriyeh, M., & Varadarajan, P. (2020). Echocardiographic evaluation of ventricular septal defects. Echocardiography, 37, 2185-2193.

[15]Stergiopulos, N., Westerhof, N., & Noble, M. I. M. (2010). Snapshots of hemodynamics: An aid for clinical research and graduate education (2nd ed.). Springer.

[16]Turner, M. E., Bouhout, I., Petit, C. J., & Kalfa, D. (2022). Transcatheter closure of atrial and ventricular septal defects: JACC focus seminar. Journal of the American College of Cardiology, 79(22), 2247-2258.